Oxygen Isotope Fractionation of O_2 Consumption Through Abiotic Photochemical Singlet Oxygen Formation Pathways

Sarah G. Pati,[*,†,‡] Lara M. Brunner,[‡] Martin Ley,[‡] and Thomas B. Hofstetter[*,¶,§]

†*Department of Environmental Geosciences, Centre for Microbiology and Environmental Systems Science, University of Vienna, 1090 Vienna, Austria*

‡*Department of Environmental Sciences, University of Basel, 4056 Basel, Switzerland*

¶*Eawag, Swiss Federal Institute of Aquatic Science and Technology, 8600 Dübendorf, Switzerland*

§*Institute of Biogeochemistry and Pollutant Dynamics (IBP), ETH Zürich, 8092 Zürich, Switzerland*

E-mail: sarah.pati@univie.ac.at; thomas.hofstetter@eawag.ch

Abstract

Oxygen isotope ratios of O_2 are important tracers for assessing biological activity in biogeochemical processes in aquatic environments. In fact, changes of $^{18}O/^{16}O$ and $^{17}O/^{16}O$ ratios of O_2 have been successfully implemented as measures for quantifying photosynthetic O_2 production and biological O_2 respiration. Despite evidence for light-dependent O_2 consumption in sunlit surface waters, however, photochemical O_2 loss processes have so far been neglected in the stable isotope-based evaluation of oxygen cycling. Here, we established the magnitude of O isotope fractionation for abiotic photochemical O_2 elimination through formation of singlet O_2, $^1O_2$, and the ensuing oxygenation and oxidation reactions with organic compounds through experiments with rose bengal as $^1O_2$ sensitizer and three different amino acids and furfuryl alcohol as chemical quenchers. Based on the kinetic analysis of light-dependent O_2 removal in the presence of different quenchers, we rationalize the observable O isotope fractionation of O_2 and the corresponding, apparent ^{18}O kinetic isotope effects (^{18}O-AKIE) with a pre-equilibrium model for the reversible formation of $^1O_2$ and its irreversible oxygenation reactions with organic compounds. While ^{18}O-AKIEs of oxygenation reactions amount to 1.03, the O isotope fractionation of O_2 vanishes systematically with increasing ratio of the rates of oxygenation reaction of $^1O_2$ vs. $^1O_2$ decay to ground state oxygen, $^3O_2$. Our findings imply that O isotope fractionation through photochemical O_2 consumption can match contributions from biological respiration at typical dissolved organic matter concentrations of lakes, rivers, and oceans and should therefore be included in future evaluations of biogeochemical O_2 cycling.

Keywords: Oxygen isotope ratio, biogeochemical O_2 cycling, photochemical oxygen activation, singlet oxygen, isotope fractionation.

Introduction

Dissolved oxygen, O_2, is a crucial chemical species in biogeochemical cycles of aquatic environments and its concentration a critical parameter used for assessing ecosystem health. Understanding the main processes affecting the dynamics of dissolved O_2 concentrations in lakes, rivers, and oceans, namely photosynthesis, respiration, and gas-water exchange, is therefore key to evaluate functions of pristine and human-impacted ecosystems.[1] The quantification of contributions of these three processes of O_2 production, consumption, and exchange to the overall O_2 cycling is difficult to achieve from the monitoring and modeling of O_2 concentration dynamics. To that end, information from the ratios of the three stable O isotopes, ^{16}O, ^{17}O, and ^{18}O, as $^{18}O/^{16}O$ and $^{17}O/^{16}O$ in so-called triple oxygen isotope analysis are increasingly exploited to disentangle contributions of the three main processes of biogeochemical O_2 cycling.[1,2]

In fact, oxygen isotope-based analyses have been successfully implemented in combination with dissolved O_2 dynamics and/or O_2-Ar ratios to quantify gross photosynthetic O_2 production, net community O_2 production, and photosynthesis rates in the (mixed) surface-layers of various ocean basins.[7–13] These isotope-based assessment of O_2 formation and consumption are based on the simplified assumption that respiration, that is the formal 4-electron reduction of O_2 to H_2O (Figure 1a), is the dominating O_2 sink term. Any other O_2 loss processes have thus far been neglected in the evaluation of O isotope ratios. However, this view is being challenged through evidence showing that in sunlit surface waters, light-dependent O_2 consumption can occur at similar or higher rates than the light-independent (i.e., "dark") respiration of O_2.[14–20] Such O_2 consumption by photochemical reactions in marine waters is estimated to be of the same magnitude as photosynthetic O_2 production by phytoplankton.[18] Light-dependent O_2 consumption can occur through biological and abiotic processes. Biological, light-dependent O_2 loss takes place through reduction of O_2 initiated by excess

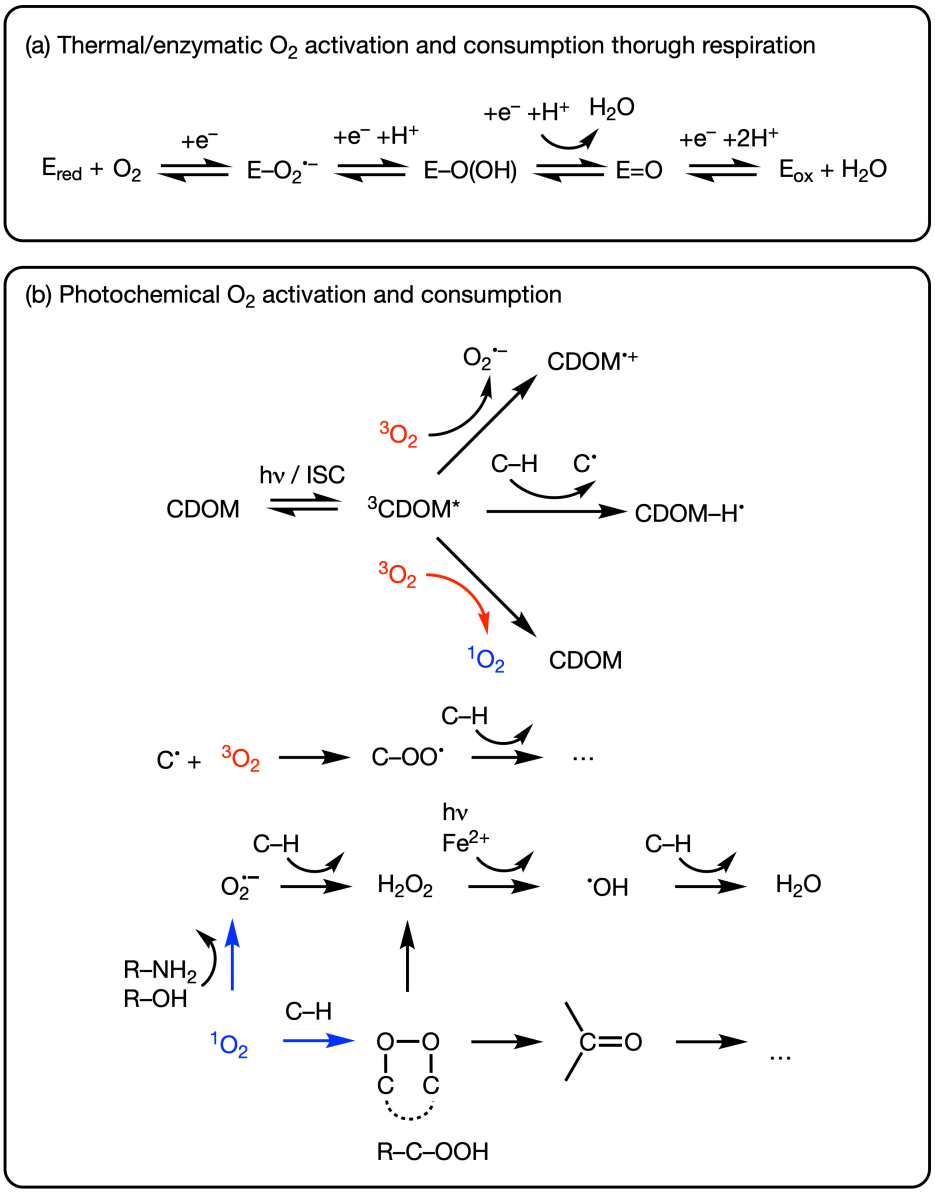

Figure 1 Schematic survey of processes and selected reaction steps responsible for O_2 consumption in aquatic environments. (a) Respiration is the enzyme-catalyzed activation of O_2 and stepwise 4-electron reduction to H_2O. Reduction equivalents for O_2 reduction from oxidation of organic substrates and cofactors are represented as electrons (e^-). (b) Abiotic photochemical O_2 consumption is shown here exemplary for processes induced by light-absorption and intersystem crossing of chromophoric dissolved organic matter (CDOM) to its excited triplet states (^{3}CDOM*). C–H and C• stand for organic compounds and carbon-centered radicals, respectively. Reactions of ^{3}CDOM* with $^3O_2$ act as source of $^1O_2$ (red arrow). $^1O_2$ loss processes contributing to photochemical O_2 consumption (blue arrows) include oxygenation of organic compounds and one-electron reduction, for example, with phenols (R-OH) and organic amines (R−NH_2), to $O_2^{\bullet-}$.[3–6]

electrons from photosystem II and, similarly to respiration, leads to the formation of water.[19,21] Abiotic, photochemical processes, by contrast, proceeds through several, chemically distinct paths of O_2 elimination (Figure 1b).

Abiotic photochemical O_2 consumption is initiated by the light-absorption of chromophoric dissolved organic matter (CDOM), nitrate, nitrite, or transition-metals and ensuing reactions with O_2. These reactions typically lead to the production of reactive oxygen species (ROS) namely singlet oxygen ($^1O_2$), superoxide ($O_2^{\bullet-}$), and hydroxyl radicals ($^\bullet OH$), as well as other transient reactive intermediates.[22] Figure 1b illustrates typical reaction sequences following the formation of triplet-excited states of CDOM ($^3CDOM^*$).[23,24] Short-lived $^3CDOM^*$ intermediates initiate a cascade of reactions that is responsible for O_2 consumption. Note that these reactions also depend on O_2 spin state. $^3CDOM^*$ reacts with ground state (triplet) dioxygen, $^3O_2$, to $O_2^{\bullet-}$, and more reduced ROS as well as with organic carbon (shown in Figure 1b as C–H) to carbon-centered radicals ($C^\bullet$). Both processes ultimately consume $^3O_2$ through formation of water and oxygenated carbon species (e.g., carbonly and alcohol species). Alternatively, reactions of $^3O_2$ with $^3CDOM^*$ results in transient $^1O_2$. $^1O_2$ species also contribute to further reductive oxygen elimination; on the one hand through oxygenation reactions such as the formation of endo- and hydroperoxides with olefinic and aromatic compounds.[25] On the other hand, $^1O_2$ enables the one-electron oxidation of organic compounds and formation of $O_2^{\bullet-}$ [3,26,27] and oxygenation of organic carbon through ROS generated from $O_2^{\bullet-}$. Abiotic photochemical O_2 consumption thus happens in a series of oxidation and oxygenation reactions that involve both $^3O_2$ and $^1O_2$ species. However, changes of O isotope ratios in O_2 from O_2 loss processes in aquatic environments have so far been determined exclusively for reactions of $^3O_2$. It therefore remains unclear whether O_2 consumption through reactions of $^1O_2$ exert any effect on the observable $^{18}O/^{16}O$ and $^{17}O/^{16}O$ ratios of O_2.

Changes of O isotope ratios of O_2, also referred to as O isotope fractionation, occur

because of kinetic isotope effects (KIEs) of (bio)chemical reactions, that is the different rate constants pertinent to the transformation of heavy (i.e., $^{18}O/^{16}O$ or $^{17}O/^{16}O$) and light ($^{16}O^{16}O$) dioxygen isotopologues. This phenomenon is quantified in terms of O isotopic enrichment factors, O-ϵ. For changes of $^{18}O/^{16}O$ ratios, for example, the ^{18}O-ϵ follows from eq 1.

$$^{18}\text{O-}\epsilon = \frac{1}{^{18}\text{O-KIE}} - 1 = \frac{1}{^{16}k/^{18}k} - 1 \tag{1}$$

where ^{16}k and ^{18}k are the rate constants for reactions of $^{16}O^{16}O$ and $^{18}O^{16}O$ isotopologues, respectively, and ^{18}O-KIE is the corresponding kinetic isotope effect. Note that the same definition applies to ^{17}O-ϵ and ^{17}O-KIE for reactions of $^{16}O^{16}O$ and $^{17}O^{16}O$ isotopologues. O-ϵ values reflect how bonds in O_2 are broken and formed and are hence specific for the type of reaction or process responsible for O_2 consumption.[28] ^{18}O-ϵ values for O_2 respiration by aquatic microbial communities, in fact, are confined to a narrow range between $-17‰$ and $-21‰$.[29–31] These numbers correspond to apparent ^{18}O-KIE of approx. 1.02. Conversely, ^{18}O-ϵ values for abiotic photochemical O_2 consumption determined with selected CDOM species of different origins amount to $-8‰$ to $-10‰$.[32,33] The apparent difference to ^{18}O-ϵ data for respiration is key to disentangle competing oxygen consumption processes in the biogeochemical O_2 cycling.

Unfortunately, contributions of reactions of $^1O_2$ to the observed ^{18}O-ϵ values for abiotic photochemical O_2 consumption were not elucidated so far. Given that the photochemistry of $^1O_2$ is well-understood,[3,22,23,34–38] the isotope fractionation of O_2 tied to the fate of $^1O_2$ can be rationalized with two main processes (Figure 1b). First, the reversible formation of $^1O_2$ from energy transfer of ^{3}CDOM* to $^3O_2$ and $^1O_2$ decay back to $^3O_2$. Second, chemical reactions of $^1O_2$ through oxygenation of susceptible moieties of CDOM or other organic compounds and $^1O_2$ reduction to $O_2^{\bullet-}$. Isotope fractionation of reactants in such pre-equilibrium kinetic regimes are well understood from studies of enzyme kinetics.[39,40] Such

analyses of pre-equilibrium kinetics and isotope fractionation allow one to postulate that the maximum observable O_2 isotope fractionation will be determined primarily by the isotope effects pertinent to $^1O_2$ loss reactions, that is oxygenation to peroxide products and electron transfer to $O_2^{\bullet-}$. However, the expression of isotope fractionation in O_2 will critically depend on the ratio of rates of $^1O_2$ decay to $^3O_2$ vs. oxygenation and electron transfer. As is known from reactions of enzymatically activated dioxygen species, such oxygenation and electron transfer reactions can exhibit substantial ^{18}O-KIEs of up to 1.05.[41–48]

The goal of this work was to explore the magnitude and variability of isotope fractionation of reactions of O_2 through photochemical formation of $^1O_2$. To that end, we studied O_2 isotope fractionation associated with the formation of $^1O_2$ and the reaction of $^1O_2$ with reactive functional groups present in dissolved organic matter in laboratory model systems with probe compounds for $^1O_2$-reactive CDOM moieties of known reactivity towards $^1O_2$. Specifically, we (i) examined the kinetics of O_2 consumption through $^1O_2$-dependent pathways to identify kinetic regimes pertinent to hypothesized processes of reversible $^1O_2$ formation vs. irreversible $^1O_2$ forward reactions. To that end, we established experimental conditions that enabled the analyses of O_2 reaction kinetics and isotope fractionating processes in experiments with rose bengal, a well-studied $^1O_2$ sensitizer, as well as three different amino acids and furfuryl alcohol as chemical quenchers of $^1O_2$,[3,49] to which we refer to in the following as probe compounds. (ii) We determined ^{18}O-ϵ values for $^1O_2$ formation from O_2 and ensuing reactions of $^1O_2$ with various probe compounds and experimental conditions. (iii) Finally, we evaluated the ^{18}O KIEs of $^1O_2$ reactions with probe compounds and discuss implications for applying O isotope analysis of O_2 for assessment of photochemical O_2 consumption.

Matherials and methods

Chemicals and solutions

Unless noted otherwise, chemicals were purchased from Sigma-Aldrich and used as received. Furfuryl alcohol (98%), L-histidine (99%), L-methionine (99.5%), and L-tyrosine (99%) were used as probe compounds and rose bengal (95%) was used as a $^1O_2$ sensitizer. Furfuryl alcohol was distilled prior to use. Sodium dihydrogen phosphate dihydrate ($NaH_2PO_4 \cdot 2\,H_2O$, 99%, Merck KGaA), dipotassium phosphate anhydrous (K_2HPO_4, 99%, Merck KGaA), hydrochloric acid (HCl, 37%, VWR Chemicals), and sodium hydroxide (NaOH, 98%) were used for making buffer solutions. Sodium sulfite anhydrous (Na_2SO_3, 98%) was used to calibrate optical oxygen sensors. All solutions were prepared in air-equilibrated ultrapure water (18.2 MΩ·cm, ELGA LabWater). He (99.999%), N_2 (99.999%), and O_2 (99.995%) were obtained from Carbagas.

Irradiation experiments

Irradiation experiments were performed in completely filled 12 mL Exetainer (15.5 mm o.d., Labco Limited) sealed with screw caps and butyl rubber septa or 12 mL crimp-top vials (22.5 mm o.d.) sealed with butyl rubber stoppers and aluminum crimp caps. All experiments were performed in 10 mM phosphate buffer at pH 7.0 (furfuryl alcohol), 7.7 (histidine), or 8.4 (methionine, tyrosine). The pH was chosen to match experimental conditions under which second-order reaction rate constants of the probe compounds with $^1O_2$ were determined.[50–52] $^1O_2$ was selectively generated by visible light irradiation of rose bengal ($0.4 - 20$ μM). A 30 W fluorescent light bulb or an overhead projector were used as an irradiation source at a distance of $10 - 40$ cm and $500 - 2000$ cm, respectively. Initial probe compound concentrations were $0.25 - 250$ mM for furfuryl alcohol, $0.15 - 100$ mM for histidine, $0.2 - 1.2$ mM for tyrosine, and $0.6 - 19$ mM for methionine. For each set of conditions, $6 - 10$

completely filled (i.e., headspace-free) and closed reactors containing buffer solution, probe compound, and rose bengal were irradiated for different amounts of time (up to 240 min) until desired final dissolved O_2 concentrations were reached. Control experiments in which no O_2 was consumed were performed without addition of rose bengal or probe compounds. Dark controls were performed with reactors wrapped in aluminum foil. All controls were irradiated for the maximum duration of a given experiment. After irradiation, dissolved O_2 concentrations were measured with an optical oxygen microsensor (PyroScience or PreSens - Precision Sensing), which was introduced into the closed reactors through a needle.[53] O_2 concentration measurements were temperature corrected and the sensors were calibrated with air-saturated water and with a 300 mM Na_2SO_3 solution.

Oxygen isotope analysis

$^{18}O/^{16}O$ ratios of dissolved O_2 were measured by gas chromatography coupled to isotope ratio mass spectrometry (GC/IRMS) as described previously.[47,54] Briefly, a headspace was created with He (5 mL liquid replaced in Exetainer) or N_2 (3 mL liquid replaced in crimp-top vials) in all reactors. Partitioning of O_2 into the gas phase was facilitated by horizontal shaking at 200 rpm for 30 min (crimp-top vials) or 60 min (Exetainer) while the vials were kept upside down. Blank samples were prepared by filling vials completely with N_2-purged water in an anaerobic glove box with a N_2 atmosphere (MBraun, residual O_2 content < 0.1 ppm or GS GLOVEBOX Systemtechnik, residual O_2 content < 1 ppm). Vials filled with air-equilibrated water and Exetainer containing 150 μL ambient air in He were used as isotopic O_2 reference standards. Blanks and standards containing water were prepared for analysis as described above for the samples from irradiation experiments. Most samples were analyzed by the GasBench/IRMS setup described in Bopp et al.[47] with a 60 m Rt-Molsieve 5Å PLOT column (Restek from BGB Analytik) at 25°C. Some samples from experiments with furfuryl alcohol were analyzed by the GC/IRMS setup described in Pati et al.[54] with

a 30 m Rt-Molsieve 5Å PLOT column at 30°C. Despite potential for Ar interference in the latter setup,[47] an identical experiment analyzed on both instruments gave identical results (see entries 3 and 4 in Table 1).

Data evaluation

$^{18}O/^{16}O$ ratios are reported as $\delta^{18}O$ values in per mil (‰, ± standard deviation) relative to Vienna Standard Mean Ocean Water (VSMOW). All $\delta^{18}O$ values were corrected for blank contributions as described in Pati et al.[54] as well as for instrument linearity (change in $\delta^{18}O$ values with signal size) and instrument drift (change in $\delta^{18}O$ values over time).[55] Instrument linearity correction was based on daily measurements of reference gas peaks with different amplitudes and instrument drift correction was based on measurements of standards evenly spread across each measurement sequence. Additionally, a one-point calibration with dilute air standards was applied assuming a $\delta^{18}O$ value of 23.8‰ for O_2 in ambient air.[56–59] We recently showed that for the range of $\delta^{18}O$ values measured in this study, such a one-point calibration provide sufficiently accurate $^{18}O/^{16}O$ ratios.[60] Corrected $\delta^{18}O$ values are reported in permil deviation (‰, ± 1 stdev) vs. VSMOW.

The magnitude of O isotope fractionation associated with O_2 consumption is reported in terms of ϵ value (in ‰, ± 95% confidence intervals), which was calculated as the slope of a linear regression according to eq 2.

$$\ln\left(\frac{\delta^{18}O+1}{\delta^{18}O_0+1}\right) = \epsilon \cdot \ln f = \left(\frac{1}{^{18}\text{O-KIE}} - 1\right) \cdot \ln\left(\frac{[O_2]}{[O_2]_0}\right) \quad (2)$$

where $\delta^{18}O_0$ and $\delta^{18}O$ are the O isotopic composition of O_2 at the beginning of an experiment and in a sample at a given fraction of remaining O_2 ($f = [O_2]/[O_2]_0$), respectively, and ^{18}O-AKIE is the apparent ^{18}O kinetic isotope effect averaged for the two O atoms in O_2.

Results and discussion

Kinetics of dissolved O_2 consumption through reactions involving $^1O_2$

We examined the kinetics of O_2 consumption through $^1O_2$-dependent pathways to identify kinetic regimes pertinent to hypothesized processes of reversible $^1O_2$ formation vs. irreversible $^1O_2$ reactions with $^1O_2$ quenchers, that is organic probe compounds as postulated in Figure 1b. Typical concentration gradients of O_2 from experiments, in which $^1O_2$ is generated with rose bengal as sensitizer and histidine is present as probe compound, are shown in Figure 2. Experimental conditions (i.e., different probe compound and rose bengal concentrations, distance to light source) were optimized for convenient sampling time intervals of approximately 10 min. Consequently, the maximum irradiation time varied between 16 and 240 min for the different experiments. Over this period, $50 - 90\%$ of the initial, dissolved O_2 (approx. 270 μM) was consumed.

Figure 2 emblematically illustrates three typical observations for experiments with histidine as probe compound. O_2 reaction kinetis were zero-order at an initial histidine concentration that exceeded that of O_2 substantially (100 mM and 0.3 mM for histidine and O_2, respectively). Conversely, O_2 consumption kinetics were pseudo-first order when similar initial concentrations of probe compound and O_2 were used. Finally, only negligible O_2 disappearance (i.e., $< (2 - 6)\%$ of the initial O_2 concentration) was observed in control experiments without rose bengal, without probe compound, and in dark controls, where vials containing both rose bengal and probe compounds were wrapped in aluminum foil, respectively. The complete compilation of experimental conditions, observed O_2 reaction order, and O_2 disappearance rate constants for experiments with different probe compounds are shown in Table 1. Note that O_2 consumption in experiments with methionine followed apparent zero order kinetics given that initial precursor compound concentrations exceeded dissolved

O_2 saturation concentration in all experimental conditions. This observation is consistent with results from experiments with elevated concentrations of other probe compounds.

We rationalized the observed reaction order of O_2 disappearance using a rate law expression in which we assume that O_2 reversibly forms $^1O_2$. The latter subsequently undergoes irreversible reaction(s) with one of the probe compounds as in eq 3.

$$O_2 \underset{k_2}{\overset{k_1[^3RB^*]_{ss}}{\rightleftharpoons}} {}^1O_2 \xrightarrow{k_3[PC]} \text{products} \tag{3}$$

where k_1, k_2, and k_3 are reaction rate constants for $^1O_2$ formation from excited triplet states of rose bengal ($^3RB^*$), the deactivation of $^1O_2$ to $^3O_2$, and any oxygenation or electron transfer reaction of $^1O_2$ with the probe compound, respectively. $[^3RB^*]_{ss}$ is the steady-state concentration of triplet-excited states of rose bengal in the irradiation experiments, and [PC] stands for the concentration of the probe compound. Note that numerical values for k_2 and

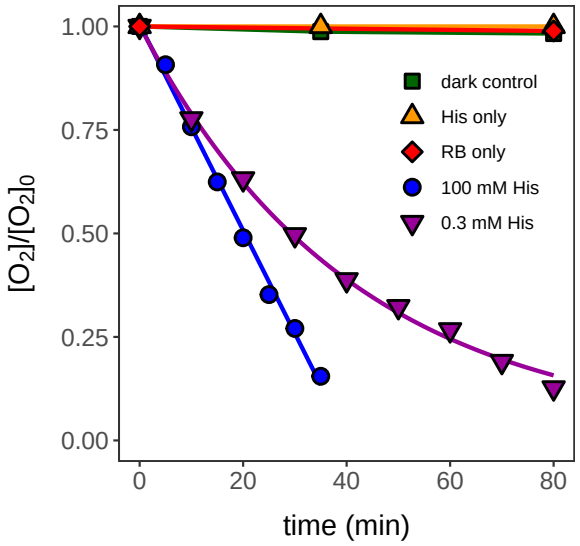

Figure 2 Normalized dissolved O_2 concentrations vs. time during irradiation experiments in aqueous solution with rose bengal (RB) and 0.3 mM histidine (His, purple downward triangles, entry 12 in Table 1), rose bengal and 100 mM histidine (blue circles, entry 5), histidine only (yellow upward triangles), rose bengal only (red diamonds), and during dark controls (green squares).

k_3 have been determined previously.[50–52,61]

Following the kinetic scheme of eq 3, the disappearance of O_2 in our experiments is given by eq 4

$$\frac{d[O_2]}{dt} = -k_1[^3RB^*][O_2] + k_2[^1O_2]_{ss} \tag{4}$$

where $[O_2]$ is the dissolved oxygen concentration and $[^1O_2]_{ss}$ is the steady-state concentration of singlet oxygen, which follows form eq 5.

$$[^1O_2]_{ss} = \frac{k_1[^3RB^*][O_2]}{k_2 + k_3[PC]} \tag{5}$$

Substitution of eq 5 into eq 4 and some rearrangements lead to eq 6. This equation allows for expressing O_2 removal in terms of the ratio of forward and backward reactions rates of $^1O_2$ ($k_3[PC]/k_2$), respectively, and thus includes the concentration of the probe compound. The latter was a key factor determining the apparent reaction order of O_2 reactivity.

$$\frac{d[O_2]}{dt} = -k_1[^3RB^*]_{ss}[O_2]\left(\frac{k_3[PC]/k_2}{1 + k_3[PC]/k_2}\right) \tag{6}$$

In our experimental setup, we can assume that the dominant quenching mechanism of $^3RB^*$ is the reaction with dissolved O_2.[23] Following the formalism used by Rosario-Ortiz and Canonica[24], $[^3RB^*]_{ss}$ is then given by eq 7.

$$[^3RB^*]_{ss} = \frac{r^f_{^3RB^*}}{k_1/\gamma_{^1O_2} \cdot [O_2]} \tag{7}$$

where $r^f_{^3RB^*}$ is the rate of $^3RB^*$ formation and $\gamma_{^1O_2}$ is the singlet oxygen formation yield for the reaction between $^3RB^*$ and dissolved O_2. Insertion of eq 7 into the rate law of O_2 consumption, eq 6, leads to eq 8 that we use here to interpret the observed reaction order.

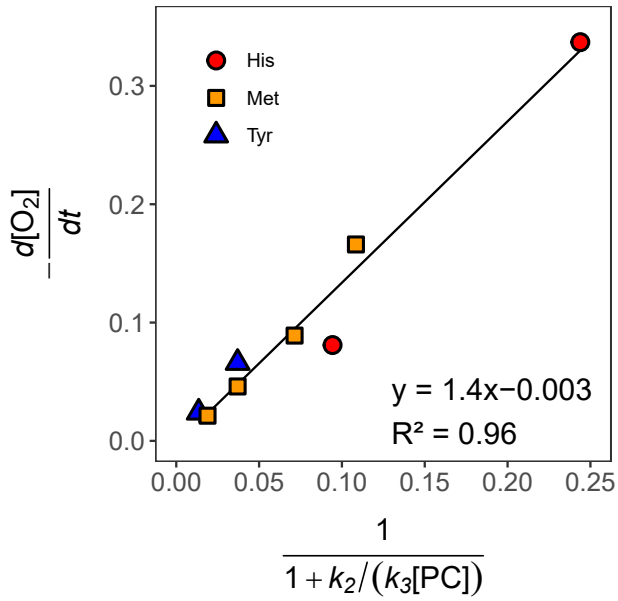

Figure 3 Linear correlation between apparent zero order rate constants and the kinetic term $1/(1+k_2/(k_3[\mathrm{PC}]))$ in experiments with histidine (His, red circles), tyrosine (Tyr, blue triangles), and methionine (Met, yellow squares) performed under similar experimental conditions (see entries 10-11, 14-15, and 18-21 in Table 1).

$$\begin{aligned}\frac{d[\mathrm{O_2}]}{dt} &= -\gamma_{^1\mathrm{O_2}} r^f_{^3\mathrm{RB}^*}\left(\frac{k_3[\mathrm{PC}]/k_2}{1+k_3[\mathrm{PC}]/k_2}\right)\\ &= -\frac{\gamma_{^1\mathrm{O_2}} r^f_{^3\mathrm{RB}^*}}{1+k_2/(k_3[\mathrm{PC}])}\end{aligned} \tag{8}$$

Note that according to eq 8, the rate of O_2 consumption is now independent of $[O_2]$. Kinetics of O_2 consumption follow zero order for large [PC] concentrations when the denominator approaches unity, that is $1 + k_2/(k_3[\mathrm{PC}]) \approx 1$. The rate of O_2 consumption is then determined by $^1O_2$ formation and equals $\gamma_{^1\mathrm{O_2}} r^f_{^3\mathrm{RB}^*}$. In fact, in all experiments with identical light conditions (fluorescent light bulb at 10 cm distance; FLB (10 cm) in Table 1) and rose bengal concentrations between 4 and 20 μM, apparent zero order rate constants linearly correlated with $1/(1 + k_2/(k_3[\mathrm{PC}]))$ as shown in Figure 3. According to eq 8, the slope

of the linear regression in Figure 3 is the rate of $^1O_2$ formation, $\gamma_{^1O_2} r^f_{^3RB^*}$, which appears constant under these experimental conditions. Apparent zero-order rate constants obtained with different light source conditions or with lower rose bengal concentrations do not show this linear correlation. This observation indicates that different rates of $^1O_2$ formation for these cases were likely due to a different $r^f_{^3RB^*}$. This interpretation of the observed O_2 disappearance supports the validity of the rate law from eq 8, when [PC] is sufficiently large to be considered constant throughout the experiment. Once [PC] becomes small, eq 8 indicates the change from zero- to first-order kinetics as we observed with probe compounds furfuryl alkohol, histidine, and tyrosine. Under these conditions, the rate of O_2 consumption is limited by reactions of $^1O_2$ with the probe compound and linearly depends on [PC]. Finally, if the initial probe compound concentrations and that of dissolved O_2 are of similar magnitude and decrease at similar rates during the course of the reaction, both $^1O_2$ formation equilibria and irreversible forward reaction with the probe compound contribute to the observed rate of O_2 disappearance. The reaction kinetics will then appear to be first order (see entries 3, 4, 12, 13, and 16 in Table 1). Collectively, the kinetic analysis with eq 8 allows for disentangling the reversible $^1O_2$ formation process and the irreversible reaction of $^1O_2$ with probe compounds. The outcome is also critical to assign any observed O isotope fractionation of O_2 to the two processes.

Isotope fractionation of dissolved O_2 through reactions with $^1O_2$

Typical trends of $\delta^{18}O$ values of dissolved O_2 during irradiation experiments with rose bengal and probe compounds are shown in Figure 4. Substantial O isotope fractionation is illustrated with histidine as probe compound at an initial concentration of 0.3 mM (entry 12, Table 1). $\delta^{18}O$ values increased from 24.5 ± 0.2‰ to 79.9 ± 0.8‰ as 87% of the initial, dissolved O_2 was consumed, corresponding to an ^{18}O-ϵ of -25.5‰. Conversely, experiments

Table 1 Experimental conditions (probe compound (PC) type and concentration, rose bengal (RB) concentration, light source, number of replicates), reaction order, rate constants, isotope fractionation (^{18}O-ϵ), and apparent ^{18}O-KIEs for all experiments conducted. [a]

Entry	PC	[PC] (mM)	[RB] (μM)	light source/ conditions [b]	replicates	kinetic order	$d[O_2]/dt$ (μM s^{-1} or (10^{-3} s^{-1}) [c]	k_3[PC]/k_2 (–)	^{18}O-ϵ (‰)	^{18}O-KIE (–)
1	FFA	250	4	OHP	3	zero-order	0.40 ± 0.07	120.	0.1 ± 0.7	0.9999 ± 0.0007
2	FFA	2.5	4	OHP	1	zero-order	0.24 ± 0.02	1.2	–17 ± 5	1.018 ± 0.005
3	FFA	0.25	4	OHP	1	first-order	0.46 ± 0.08	0.12	–23 ± 3	1.023 ± 0.004
4	FFA	0.26	10	FLB (10 cm)	1	first-order	0.56 ± 0.05	0.13	–23 ± 1	1.024 ± 0.002
5	His	100	0.4	FLB (20 cm)	1	zero-order	0.103 ± 0.006	26.	–3.9 ± 0.5	1.0039 ± 0.0005
6	His	40	4	FLB (40 cm)	2	zero-order	0.180 ± 0.007	10.	–7.7 ± 0.4	1.0078 ± 0.0004
7	His	15	0.5	FLB (20 cm)	1	zero-order	0.099 ± 0.008	3.8	–11.3 ± 0.8	1.0114 ± 0.0008
8	His	5.0	1	FLB (20 cm)	1	zero-order	0.138 ± 0.008	1.3	–18.5 ± 0.6	1.0189 ± 0.0006
9	His	4.0	4	FLB (20 cm)	4	zero-order	0.21 ± 0.01	1.0	–18.6 ± 0.6	1.0189 ± 0.0007
10	His	1.3	8	FLB (10 cm)	1	zero-order	0.34 ± 0.04	0.32	–20 ± 1	1.021 ± 0.001
11	His	0.40	4	FLB (10 cm)	5	zero-order	0.081 ± 0.003	0.10	–23.5 ± 0.4	1.0240 ± 0.0004
12	His	0.30	10	FLB (10 cm)	3	first-order	0.43 ± 0.03	0.077	–25.2 ± 0.4	1.0258 ± 0.0004
13	His	0.15	20	FLB (10 cm)	1	first-order	0.17 ± 0.02	0.038	–25 ± 2	1.026 ± 0.002
14	Tyr	1.2	20	FLB (10 cm)	3	zero-order	0.066 ± 0.005	0.038	–26.7 ± 0.9	1.0275 ± 0.0009
15	Tyr	0.43	20	FLB (10 cm)	2	zero-order	0.024 ± 0.001	0.014	–25 ± 1	1.025 ± 0.001
16	Tyr	0.20	20	FLB (10 cm)	2	first-order	0.061 ± 0.004	0.0064	–23.5 ± 0.5	1.0240 ± 0.0006
17	Met	19	1	FLB (10 cm)	2	zero-order	0.189 ± 0.006	1.2	–24.3 ± 0.8	1.0249 ± 0.0009
18	Met	1.9	10	FLB (10 cm)	1	zero-order	0.166 ± 0.008	0.12	–28.7 ± 0.7	1.0295 ± 0.0007
19	Met	1.2	10	FLB (10 cm)	2	zero-order	0.089 ± 0.003	0.077	–28.4 ± 0.9	1.029 ± 0.001
20	Met	0.6	20	FLB (10 cm)	3	zero-order	0.046 ± 0.003	0.038	–28 ± 1	1.029 ± 0.001
21	Met	0.3	20	FLB (10 cm)	1	zero-order	0.0213 ± 0.0009	0.019	–30 ± 1	1.031 ± 0.001

[a] Errors are given as 95% confidence intervals;

[b] OHP: overhead projector at variable distances, FLB: fluorescent light bulb at fixed distance;

[c] μM s^{-1} for zero-order kinetics and s^{-1} for pseudo-first order kinetics.

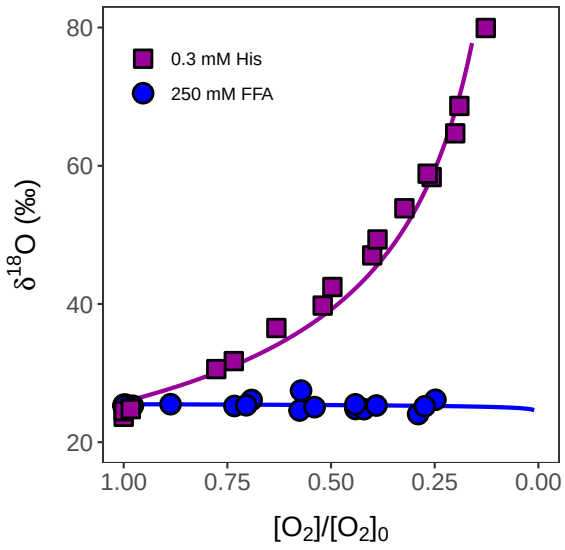

Figure 4 Change in δ^{18}O values vs. fraction of remaining O_2 concentration ($[O_2]/[O_2]_0$) during irradiation experiments with rose bengal and 0.3 mM histdine (His, purple squares, entry 12 in Table 1) and 250 mM furfuryl alcohol (FFA, blue circles, entry 1).

with furfuryl alcohol as probe compound at an initial concentration of 250 mM revealed only minor O isotope fractionation, that is a change in δ^{18}O values from 25.3‰ to 27.5‰ despite a similar degree of O_2 consumption (entry 3, Table 1). Note that the maximum change of δ^{18}O observed in a control experiment was 0.7‰ which we use as lower bound for negligible isotope fractionation comparison. To that end, all of the photochemical experiments shown here reveal some extent of O isotope fractionation which we can thus ascribe to the reaction of dissolved O_2 with triplet excited states of rose bengal, the formation of singlet oxygen, and the subsequent reaction between $^1O_2$ and probe compounds.

The data in Table 1 shows that O isotope fractionation and thus ^{18}O-ϵ varies substantially from no fractionation (0.1 ± 0.7)‰ to -30‰ for all probe compounds studied. As a general trend, O isotope fractionation increases (i.e., ^{18}O-ϵ values become more negative) with decreasing initial probe compound concentration. The extent of O isotope fractionation, however, did not correlate with reaction order. An interpretation of the observed trends of ^{18}O-ϵ values follows from the evaluation of isotope effects pertinent to the elementary

reaction steps of O_2 activation to $^1O_2$ and its reaction with the probe compounds outlined in eq 3.

Derivation of isotope effects associated with the formation and reactions of $^1O_2$

We derived the isotope effects of $^1O_2$ formation and subsequent oxygenation or electron transfer reactions from the isotopic expression of eq 6 as documented in Section S1 of the Supporting Information. To that end, we consider the ratio of O_2 isotopologue disappearance for the two most abundant isotopologues, $^{16}O^{16}O$ and $^{18}O^{16}O$, to obtain the apparent ^{18}O-kinetic isotope effect, ^{18}O-AKIE, in eq 10 from the ratio of the apparent rate constants $^{16}k_{obs}$ and $^{18}k_{obs}$.

$$\frac{d[^{16}O^{16}O]/dt}{d[^{18}O^{16}O]/dt} = \frac{^{16}k_{obs}}{^{18}k_{obs}} \cdot \frac{[^{16}O^{16}O]}{[^{18}O^{16}O]} \tag{9}$$

$$^{18}\text{O-AKIE} = \frac{^{16}k_{obs}}{^{18}k_{obs}} = \frac{\text{EIE}_1 \cdot \text{KIE}_3 + \text{KIE}_1 \cdot k_3[\text{PC}]/k_2}{1 + k_3[\text{PC}]/k_2} \tag{10}$$

where $[^{16}O^{16}O]$ and $[^{18}O^{16}O]$ are the considered isotopologue concentrations, respectively, subscripts 1 to 3 denote the elementary processes from eq 6 devided by $[O_2]$, EIE_1 is the equilibrium isotope effect of the reversible $^1O_2$ formation. KIE_1 and KIE_3 are the kinetic isotope effect of $^1O_2$ formation and the irreversible reaction of $^1O_2$ with the probe compound. $k_3[PC]/k_2$ describes the ratio of the forward and backward reaction of $^1O_2$ and therefore the relevance of reactions with probe compounds for elimination of O_2. The right-hand term in eq 10 is typical for describing the modulation of isotope effects in enzymatic pre-equilibrium kinetics where $k_3[PC]/k_2$ would be equivalent to a (forward) commitment factor in a catalytic

reaction.[39,40]

We converted the observable O isotope fractionation which one quantifies with ^{18}O-ϵ into ^{18}O-AKIE values by making use of the different reactivity of the probe compounds with $^1O_2$. Under conditions that favour $^1O_2$ elimination through reactions with the probe compounds, that is at high k_3[PC]/k_2, eq 10 simplifies to KIE_1. As shown in experiments with high furfuryl alcohol concentration where k_3[PC]/k_2 = 120 (entry 1 in Table 1), the ^{18}O-AKIE then corresponds to unity and indicates the absence of O isotope fractionation. This observation implies that KIE_1 also corresponds to 1.0. This interpretation is supported by the fact that O isotope fractionation of O_2 reaction with minor oxygen bonding changes, as in the formation of $^1O_2$, are indeed small and EIE_1, KIE_1, and KIE_2 values equal to unity.[42] Finally, KIE_1, KIE_2, and therefore EIE_1 are likely identical and independent of the reaction with any of the probe compounds in our experiments because only O_2, rose bengal, and water are involved in the first reaction step leading to $^1O_2$ formation and decay (see eq 3). Following this logic, we are able to deduce the magnitunde of KIE_3 from experiments where k_3[PC]/$k_2 \ll 1$ and ^{18}O-AKIE then corresponds to KIE_3.

Magnitude of apparent kinetic isotope effects of O_2 consumption through the photochemical $^1O_2$-formation pathway

The ^{18}O-AKIE values derived from ^{18}O-ϵ with eq 2 of the experiments shown in Table 1 are plotted in Figure 5 vs. the ratio of forward and backward reactions of $^1O_2$, k_3[PC]/k_2. Regardless of the experimental conditions and probe compounds used for quenching $^1O_2$, ^{18}O-AKIE values follow the general trend outlined in eq 10 with the assumption that the reversible formation of $^1O_2$ from the reaction of O_2 with $^3RB^*$ does not exhibit O isotope fractionation. Therefore, isotope effects associated with O_2 disappearance reflect the reaction of $^1O_2$ with the probe compounds. The O isotope fractionation of O_2 of these reactions are

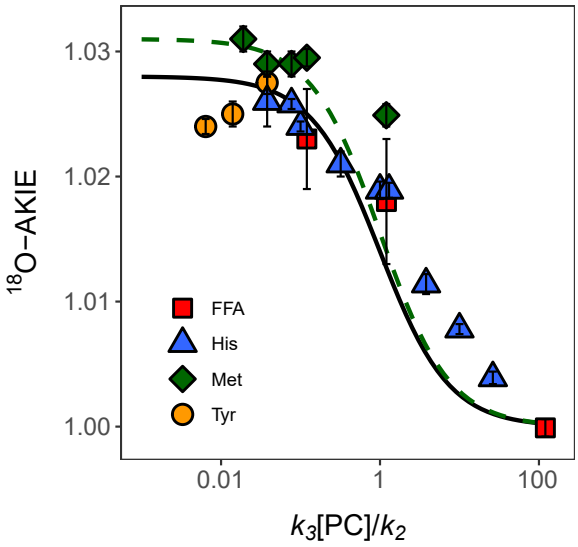

Figure 5 Apparent ^{18}O-KIEs vs. $k_3[\mathrm{PC}]/k_2$ (see Table 1) from experiments with furfuryl alcohol (FFA, red squares), histidine (His, blue triangles), methionine (Met, green diamonds), and tyrosine (Tyr, yellow circles). The black solid and green dashed lines were calculated with eq 10, a KIE_1 of 1, and KIE_3 values of 1.028 and 1.031, respectively. Note that the x-axis has a logarithmic scale for improved resolution of the data points.

masked (i.e., ^{18}O-AKIE ≈ 1) at high $k_3[\mathrm{PC}]/k_2$, that is in kinetic regimes of so-called forward commitment, where the forward reaction of $^1\mathrm{O}_2$ out-competes its decay to O_2. Conversely, ^{18}O-AKIE values approach a maximum value of 1.028 and 1.031 (solid and dashed lines in Figure 5) and thus the intrinsic kinetic isotope effect (KIE_3) when the $^1\mathrm{O}_2$ formation/decay equilibrium is faster than $^1\mathrm{O}_2$ oxygenation and electron transfer.

We note, however, small deviations of this general trend for the different probe compounds used. In experiments with methionine, ^{18}O-AKIEs approach a higher intrinsic KIE_3 of 1.031 (dashed line in Figure 5) than with histidine (1.026, solid line). ^{18}O-AKIEs from experiments with tyrosine even decrease slightly from 1.0275 to 1.0240 as forward commitment decreases. Data for ^{18}O-AKIEs for furfuryl alcohol, unfortunately, only extent do $k_3[\mathrm{PC}]/k_2$ of 0.12 and thus do not allow for observation of the maximum O isotope fractionation. Moreover, some ^{18}O-AKIEs from reactions with histidine and methionine are approximately 0.002 to 0.003

AKIE units higher than rationalized with eq 10 for $k_3[PC]/k_2$ values between 0.3 and 10. We hypothesize that the observed deviations from trends rationalized by eq 10 have two possible origins; distinct reaction mechanisms of $^1O_2$ attack at the probe compounds and, possibly, different concentrations of $^1O_2$ across the various experiments.

In fact, based on isotopic pre-equilibrium models underlying eq 10, we assume constant concentrations of $^1O_2$ and $^3RB^*$ over the course of an experiment, reactions of O_2 and $^3RB^*$ as predominant $^3RB^*$ quenching mechanism, as well as a constant rate of formation of $^3RB^*$ and a constant $^1O_2$ formation yield. Given that the rose bengal concentrations varied between 0.5 and 20 μM, the assumptions implied in the pre-equilibrium model are likely not strictly valid for all experimental conditions. The ensuing differences in reaction kinetics could be potential sources of the observed variations of ^{18}O-AKIE values.

Histidine, tyrosine, and furfuryl alcohol share a common initial reaction step through cycloaddition of $^1O_2$ to the imidazole, phenyl, and furan moieties of the probe compounds.[38,52] It is thus reasonable to assume that the similar ^{18}O-AKIE values for O_2 consumption and consistent trends with $k_3[PC]/k_2$ originate from an intrinsic KIE_3 of similar magnitude within the uncertainty of 0.003 AKIE-units identified here (Figure 5). ^{18}O-AKIEs from experiments with methionine, by contrast, are offset from the other three probe compounds. One possible explanation for this offset is that the initial reaction step of methionine with $^1O_2$ is indeed different. Methionine reacts with $^1O_2$ to a persulfoxide species,[38] where only one O atom of $^1O_2$ participates in S–O bond formation instead of both O atoms in cycloaddition mechanisms. Such correlations of decreasing changes in O bond order with decreasing experimental and theoretical O isotope effects have been established for thermal reduction reactions of O_2.[41] Moreover, the maximum AKIE determined in experiments with methionine (1.031, entry 21 in Table 1) is in good agreement with the calculated equilibrium isotope effect for O_2 reduction to HO_2^- of 1.034.[41] Unfortunately, isotope effect calculations for $^1O_2$ additions to olefins, which might provide estimates for ^{18}O AKIE values for experiments

with tyrosine, have been restricted to C and H isotopes of the olefinic probe compounds.[62] A comparison of our data with theoretical ^{18}O isotope effects for $^1O_2$ reactions is thus not possible. Regardless of the limited availability of theoretical isotope effect data for comparison, the reaction mechanisms leading to the oxygenation of the studied probe compounds with $^1O_2$ are more complicated than the single rate-limiting step assumed here and a likely source of AKIE variability.

Conclusions

Our data show that photochemical O_2 consumption through pathways involving $^1O_2$ can lead to significant O isotope fractionation that originates from oxygenation reactions of organic compounds with $^1O_2$. In surface waters, such compounds are present as reactive structural moieties of DOM. The magnitude of isotope fractionation of dissolved O_2 will thus dependent on the concentration, type, and accessibility of reactive DOM moieties. At high concentrations of DOM or $^1O_2$-reactive moieties therein, we expect a similar masking of O kinetic isotope effects through fast reactions of $^1O_2$ that would result in only neglible, observable O isotope fractionation of dissolved O_2. With decreasing concentrations of reactive functional groups, ^{18}O-ϵ values of dissolved O_2 will increase to up to $-27‰$ to $-30‰$ once the concentration of furan, imidazole, phenol, and sulfide moieties become kinetically limiting. This increase in O isotope fractionation of dissolved O_2 is caused by a shift in the rate-limiting step of the overall reaction from the formation of $^1O_2$ (no isotope fractionation) to the oxygenation and eletron transfer reaction between $^1O_2$ and organic moieties.

In natural aquatic systems, the most abundant $^1O_2$-reactive functional group are phenols with concentrations in terrestrial dissolved organic matter of $2-4$ mmol g^{-1} C.[63] With typical dissolved organic carbon concentrations of $0.5-3$ mg L^{-1} for oceans and $0.5-50$ mg L^{-1} for lakes and rivers,[64] total phenol concentrations range between 1 and 200 μM. Even

though 200 μM is the lowest phenol concentration used in this study, photochemical O_2 consumption through $^1O_2$ formation will only be relevant at elevated phenol concentrations. Therefore, isotope fractionation associated with photochemical O_2 consumption due to $^1O_2$ formation can be expected to be close to the -24‰ determined with 200 μM tyrosine. Consequently, isotope fractionation of photochemical O_2 consumption through $^1O_2$ formation differs from isotope fractionation of respiration. This comparison implies that photochemical O_2 consumption should be integrated as part of the assessment of gross photosynthetic O_2 production and net community O_2 production through the evaluation of (triple) oxygen isotope fractionation of O_2. Before doing so, however, the isotope fractionation of additional photochemical consumption pathways also need to be assessed. This becomes particularly obvious when comparing the range of isotope fractionation determined in this study for $^1O_2$ formation specifically (0‰ to -30‰) and previously for overall photochemical O_2 consumption (-8‰ to -10‰).[32,33] This comparison suggests that $^1O_2$ formation might not be the dominant pathway for photochemical O_2 consumption in complex CDOM mixtures.

Conflicts of interest

There are no conflicts to declare.

Acknowledgements

This work was supported by the Swiss National Science Foundation (Grant no. PZ00P2_186083). We thank Moritz Lehmann and Thomas Kuhn for facilitating and supporting IRMS measurements.

References

(1) Mader, M.; Schmidt, C.; van Geldern, R.; Barth, J. A. C. Dissolved oxygen in water and its stable isotope effects: A review. *Chem. Geol.* **2017**, *473*, 10–21.

(2) Juranek, L. W.; Quay, P. D. Using triple isotopes of dissolved oxygen to evaluate global marine productivity. *Annu. Rev. Mar. Sci.* **2013**, *5*, 503–524.

(3) Barrios, B.; Mohrhardt, B.; Doskey, P. V.; Minakata, D. Mechanistic insight into the reactivities of aqueous-phase singlet oxygen with organic compounds. *Environ. Sci. Technol.* **2021**, *55*, 8054–8067.

(4) Al-Nu'airat, J.; Dlugogorski, B. Z.; Gao, X.; Zeinali, N.; Skut, J.; Westmoreland, P. R.; Oluwoye, I.; Altarawneh, M. Reaction of phenol with singlet oxygen. *Phys. Chem. Chem. Phys.* **2018**, *21*, 171–183.

(5) Méndez-Hurtado, J.; López, R.; Suárez, D.; Menéndez, M. I. Theoretical study of the oxidation of histidine by singlet oxygen. *Chemistry - A European Journal* **2012**, *18*, 8437–8447.

(6) Braun, A.; Dahn, H.; Gassmann, E.; Gerothanassis, I.; Jakob, L.; Kateva, J.; Martinez, C. G.; Oliveros, E. (2 + 4)-Cycloaddition with singlet oxygen. ^{17}O-lnvestigation of the reactivity of furfuryl alcohol endoperoxide. *Photochemistry and Photobiology* **1999**, *70*, 868–874.

(7) Luz, B.; Barkan, E. Assessment of oceanic productivity with the triple-isotope composition of dissolved oxygen. *Science* **2000**, *288*, 2028–2031.

(8) Stanley, R. H.; Kirkpatrick, J. B.; Cassar, N.; Barnett, B. A.; Bender, M. L. Net community production and gross primary production rates in the western equatorial Pacific. *Global Biogeochem. Cycles* **2010**, *24*, GB4001.

(9) Juranek, L. W.; Quay, P. D.; Feely, R. A.; Lockwood, D.; Karl, D. M.; Church, M. J. Biological production in the NE Pacific and its influence on air-sea CO_2 flux: Evidence from dissolved oxygen isotopes and O_2/Ar. *J. Geophys. Res. Oceans* **2012**, *117*, C05022.

(10) Quay, P.; Stutsman, J.; Steinhoff, T. Primary production and carbon export rates across the subpolar N. Atlantic Ocean basin based on triple oxygen isotope and dissolved O_2 and Ar gas measurements. *Global Biogeochem. Cycles* **2012**, *26*, GB2003.

(11) Munro, D. R.; Quay, P. D.; Juranek, L. W.; Goericke, R. Biological production rates off the Southern California coast estimated from triple O_2 isotopes and O_2:Ar gas ratios. *Limnol. Oceanogr.* **2013**, *58*, 1312–1328.

(12) Rafelski, L. E.; Paplawsky, B.; Keeling, R. F. Continuous measurements of dissolved O_2 and oxygen isotopes in the Southern California coastal ocean. *Mar. Chem.* **2015**, *174*, 94–102.

(13) Zhu, Z.; Wang, J.; Zhang, G.; Liu, S.; Zheng, S.; Sun, X.; Xu, D.; Zhou, M. Using triple oxygen isotopes and oxygen-argon ratio to quantify ecosystem production in the mixed layer of northern South China Sea slope region. *Acta Oceanol. Sin.* **2021**, *40*, 1–15.

(14) Amon, R. M. W.; Benner, R. Photochemical and microbial consumption of dissolved organic carbon and dissolved oxygen in the Amazon River system. *Geochim. Cosmochim. Acta* **1996**, *60*, 1783–1792.

(15) Reitner, B.; Herndl, G. J.; Herzig, A. Role of ultraviolet-B radiation on photochemical and microbial oxygen consumption in a humic-rich shallow lake. *Limnol. Oceanogr.* **1997**, *42*, 950–960.

(16) Obernosterer, I.; Ruardij, P.; Herndl, G. J. Spatial and diurnal dynamics of dissolved organic matter (DOM) fluorescence and H_2O_2 and the photochemical oxygen demand

of surface water DOM across the subtropical Atlantic Ocean. *Limnol. Oceanogr.* **2001**, *46*, 632–643.

(17) Kitidis, V.; Tilstone, G. H.; Serret, P.; Smyth, T. J.; Torres, R.; Robinson, C. Oxygen photolysis in the Mauritanian upwelling: Implications for net community production. *Limnol. Oceanogr.* **2014**, *59*, 299–310.

(18) Gieskes, W. W. C.; Laane, R. W. P. M.; Ruardij, P. Photo-oxidation: Major sink of oxygen in the ocean surface layer. *Mar. Chem.* **2015**, *177*, 472–475.

(19) Bailleul, B.; Park, J.; Brown, C. M.; Bidle, K. D.; Lee, S. H.; Falkowski, P. G. Direct measurements of the light dependence of gross photosynthesis and oxygen consumption in the ocean. *Limnol. Oceanogr.* **2017**, *62*, 1066–1079.

(20) Howard, E. M.; Spivak, A. C.; Karolewski, J. S.; Gosselin, K. M.; Sandwith, Z. O.; Manning, C. C.; Stanley, R. H. Oxygen and triple oxygen isotope measurements provide different insights into gross oxygen production in a shallow salt marsh pond. *Estuar. Coast.* **2020**, *43*, 1908–1922.

(21) The dynamics of photosynthesis. *Annu. Rev. Genet.* **2008**, *42*, 463–515.

(22) Blough, N. V.; Zepp, R. G. In *Active Oxygen in Chemistry*; Foote, C. S., Valentine, J. S., Greenberg, A., Liebman, J. F., Eds.; 1995; pp 280–333.

(23) McNeill, K.; Canonica, S. Triplet state dissolved organic matter in aquatic photochemistry: reaction mechanisms, substrate scope, and photophysical properties. *Environ. Sci.: Process. Impacts* **2016**, *18*, 1381–1399.

(24) Rosario-Ortiz, F. L.; Canonica, S. Probe compounds to assess the photochemical activity of dissolved organic matter. *Environ. Sci. Technol.* **2016**, *50*, 12532–12547.

(25) Greer, A. Christopher Foote's discovery of the role of singlet oxygen [$^1O_2$ ($^1\Delta_g$)] in photosensitized oxidation reactions. *Acc. Chem. Res.* **2006**, *39*, 797–804.

(26) Saito, I.; Matsuura, T.; Inoue, K. Formation of superoxide ion via one-electron transfer from electron donors to singlet oxygen. *J. Am. Chem. Soc.* **1983**, *105*, 3200–3206.

(27) Saito, I.; Matsuura, T.; Inoue, K. Formation of superoxideion from singlet oxygen. Use of a water-soluble singlet oxygen source. *J. Am. Chem. Soc.* **1981**, *103*, 188–190.

(28) Scott, K. M.; Lu, X.; Cavanaugh, C. M.; Liu, J. S. Optimal methods for estimating kinetic isotope effects from different forms of the Rayleigh distillation equation. *Geochim. Cosmochim. Acta* **2004**, *68*, 433–442.

(29) Kiddon, J.; Bender, M. L.; Orchardo, J.; Caron, D. A.; Goldman, J. C.; Dennett, M. Isotopic fractionation of oxygen by respiring marine organisms. *Global Biogeochem. Cycles* **1993**, *7*, 679–694.

(30) Helman, Y.; Barkan, E.; Eisenstadt, D.; Luz, B.; Kaplan, A. Fractionation of the three stable oxygen isotopes by oxygen-producing and oxygen-consuming reactions in photosynthetic organisms. *Plant Physiol.* **2005**, *138*, 2292–2298.

(31) Ash, J. L.; Hu, H.; Yeung, L. Y. What fractionates oxygen isotopes during respiration? Insights from multiple isotopologue measurements and theory. *ACS Earth Space Chem.* **2019**, *4*, 50–66.

(32) Chomicki, K. M.; Schiff, S. L. Stable oxygen isotopic fractionation during photolytic O_2 consumption in stream waters. *Sci. Total Environ.* **2008**, *404*, 236–244.

(33) Ward, C. P.; Sharpless, C. M.; Valentine, D. L.; Aeppli, C.; Sutherland, K. M.; Wankel, S. D.; Reddy, C. M. Oxygen isotopes ($d^{18}O$) trace photochemical hydrocarbon oxidation at the sea surface. *Geophys. Res. Lett.* **2019**, *46*, 6745–6754.

(34) Ossola, R.; Jönsson, O. M.; Moor, K.; McNeill, K. Singlet oxygen quantum yields in environmental waters. *Chem. Rev.* **2021**, *121*, 4100–4146.

(35) McKay, G.; Couch, K. D.; Mezyk, S. P.; Rosario-Ortiz, F. L. Investigation of the coupled effects of molecular weight and charge-transfer interactions on the optical and photochemical properties of dissolved organic matter. *Environ. Sci. Technol.* **2016**, *50*, 8093–8102.

(36) Berg, S. M.; Whiting, Q. T.; Herrli, J. A.; Winkels, R.; Wammer, K. H.; Remucal, C. K. The role of dissolved organic matter composition in determining photochemical reactivity at the molecular level. *Environ. Sci. Technol.* **2019**, *53*, 11725–11734.

(37) Haag, W. R.; Hoigne, J. Singlet oxygen in surface waters. 3. Photochemical formation and steady-state concentrations in various types of waters. *Environ. Sci. Technol.* **1986**, *20*, 341–348.

(38) Di Mascio, P.; Martinez, G. R.; Miyamoto, S.; Ronsein, G. E.; Medeiros, M. H. G.; Cadet, J. Singlet molecular oxygen reactions with nucleic acids, lipids, and proteins. *Chem. Rev.* **2019**, *119*, 2043–2086.

(39) Cook, P. F.; Cleland, W. W. *Enzyme Kinetics and Mechanism*; Garland Science: New York, 416 pp., 2007.

(40) Northrop, D. B. The expression of isotope effects on enzyme-catalyzed reactions. *Annu. Rev. Biochem.* **1981**, *50*, 103–131.

(41) Roth, J. P.; Klinman, J. P. In *Isotope Effects in Chemistry and Biology*; Kohen, A., Limbach, H.-H., Eds.; CRC Press / Taylor & Francis: New York, 2006; pp 645–669.

(42) Roth, J. P. Oxygen isotope effects as probes of electron transfer mechanisms and structures of activated O_2. *Acc. Chem. Res.* **2009**, *42*, 399–408.

(43) Ashley, D. C.; Brinkley, D. W.; Roth, J. P. Oxygen isotope effects as structural and mechanistic probes in inorganic oxidation chemistry. *Inorg. Chem.* **2010**, *49*, 3661–3675.

(44) Bopp, C. E.; Bernet, N. M.; Meyer, F.; Khan, R.; Kohler, H.-P. E.; Buller, R.; Hofstetter, T. B. Elucidating the role of O_2 uncoupling for the adaptation of bacterial biodegradation reactions catalyzed by Rieske Oxygenases. *ACS Environmental Au* **2024**, *4*, 204–218.

(45) Bopp, C. E.; Bernet, N. M.; Kohler, H.-P. E.; Hofstetter, T. B. Elucidating the role of O_2 uncoupling in the oxidative biodegradation of organic contaminants by Rieske non-heme iron dioxygenases. *ACS Environmental Au* **2022**, *2*, 428–440.

(46) Pati, S. G.; Bopp, C. E.; Kohler, H.-P. E.; Hofstetter, T. B. Substrate-specific coupling of O_2 activation to hydroxylations of aromatic compounds by Rieske non-heme iron dioxygenases. *ACS Catal.* **2022**, *12*, 6444–6456.

(47) Bopp, C. E.; Bolotin, J.; Pati, S. G.; Hofstetter, T. B. Managing argon interference during measurements of $^{18}O/^{16}O$ ratios in O_2 by continuous-flow isotope ratio mass spectrometry. *Anal. Bioanal. Chem.* **2022**, *414*, 6177–6186.

(48) Cheah, M. H.; Millar, A. H.; Myers, R. C.; Day, D. A.; Roth, J.; Hillier, W.; Badger, M. R. Online Oxygen Kinetic Isotope Effects Using Membrane Inlet Mass Spectrometry Can Differentiate between Oxidases for Mechanistic Studies and Calculation of Their Contributions to Oxygen Consumption in Whole Tissues. *Anal. Chem.* **2014**, *86*, 5171–5178.

(49) Remucal, C. K.; McNeill, K. Photosensitized amino acid degradation in the presence of riboflavin and Its derivatives. *Environ. Sci. Technol.* **2011**, *45*, 5230–5237.

(50) Chu, C.; Lundeen, R. A.; Remucal, C. K.; Sander, M.; McNeill, K. Enhanced indi-

rect photochemical transformation of histidine and histamine through association with chromophoric dissolved organic matter. *Environ. Sci. Technol.* **2015**, *49*, 5511–5519.

(51) Matheson, I. B. C.; Lee, J. Chemical reaction rates of amino acids with singlet oxygen. *Photochem. Photobiol.* **1979**, *29*, 879–881.

(52) Haag, W. R.; Hoigné, J.; Gassman, E.; Braun, A. M. Singlet oxygen in surface waters–Part I: Furfuryl alcohol as a trapping agent. *Chemosphere* **1984**, *13*, 631–640.

(53) Pati, S. G.; Kohler, H.-P. E.; Hofstetter, T. B.; Characterization of substrate, co-substrate, and product isotope effects associated with enzymatic oxygenations of organic compounds based on compound-specific isotope analysis In *Measurement and Analysis of Kinetic Isotope Effects*; Harris, M. E., Anderson, V. E., Eds.; Methods in Enzymlology; Academic Press, 2017; Vol. 596; pp 292–329.

(54) Pati, S. G.; Bolotin, J.; Brennwald, M. S.; Kohler, H.-P. E.; Werner, R. A.; Hofstetter, T. B. Measurement of oxygen isotope ratios ($^{18}O/^{16}O$) of aqueous O_2 in small samples by gas chromatography/isotope ratio mass spectrometry. *Rapid Commun. Mass Spectrom.* **2016**, *30*, 684–690.

(55) Werner, R. A.; Brand, W. A. Referencing strategies and techniques in stable isotope ratio analysis. *Rapid Commun. Mass Spectrom.* **2001**, *15*, 501–519.

(56) Barkan, E.; Luz, B. The relationships among the three stable isotopes of oxygen in air, seawater and marine photosynthesis. *Rapid Commun. Mass Spectrom.* **2011**, *25*, 2367–2369.

(57) Pack, A.; Höweling, A.; Hezel, D. C.; Stefanak, M. T.; Beck, A.-K.; Peters, S.; Sengupta, S.; Herwartz, D.; Folco, L. Tracing the oxygen isotope composition of the upper Earth's atmosphere using cosmic spherules. *Nat. Commun.* **2017**, *8*, 15702.

(58) Laskar, A. H.; Peethambaran, R.; Adnew, G. A.; Röckmann, T. Measurement of $^{18}O^{18}O$ and $^{17}O^{18}O$ in atmospheric O_2 using the 253 Ultra mass spectrometer and applications to stratospheric and tropospheric air samples. *Rapid Commun. Mass Spectrom.* **2019**, *33*, 981–994.

(59) Wostbrock, J. A.; Cano, E. J.; Sharp, Z. D. An internally consistent triple oxygen isotope calibration of standards for silicates, carbonates and air relative to VSMOW2 and SLAP2. *Chem. Geol.* **2020**, *533*, 119432.

(60) de Carvalho, C. F. M.; Lehmann, M. F.; Pati, S. G. Improving the accuracy of $d^{18}O$ and $d^{17}O$ values of O_2 measured by continuous-flow isotope-ratio mass spectrometry with a multi-point isotope-ratio calibration. *Rapid Commun. Mass Spectrom.* **2023**, submitted.

(61) Rodgers, M. A. J.; Snowden, P. T. Lifetime of O_2 (^1D_g) in liquid water as determined by time-resolved infrared luminescence measurements. *J. Am. Chem. Soc.* **1982**, *104*, 5541–5543.

(62) Singleton, C., D. A. andn Hang; Szymanski, M. J.; Leach, A. G.; Kuwata, K. T.; Chen, J. S.; Greer, A.; Foote, C. S.; Houk, K. N. Mechanism of Ene Reactions of Singlet Oxygen. A Two-Step No-Intermediate Mechanism. *J. Am. Chem. Soc.* **2013**, *125*, 1319–1328.

(63) Houska, J.; Salhi, E.; Walpen, N.; von Gunten, U. Oxidant-reactive carbonous moieties in dissolved organic matter: Selective quantification by oxidative titration using chlorine dioxide and ozone. *Water Res.* **2021**, *207*, 117790.

(64) Mulholland, P. J. In *Aquatic Ecosystems*; Findlay, S. E. G., Sinsabaugh, R. L., Eds.; Aquatic Ecology; Academic Press: Burlington, 2003; pp 139–159.